The Optimal Porosity of Shelterbelts in an Oasis–Desert Ecotone in the Junggar Basin, Xinjiang, China

Qinming Sun[1, 2, 3], Tong Liu[2*], Manhou Xu[4] and Zhiquan Han[2]

[1]Agricultural College, Shihezi University, Shihezi 832003, China

[2]College of Life Sciences, Shihezi University, Shihezi 832003, China

[3]Key Laboratory of Special Fruits & Vegetables Cultivation Physiology and Germplasm Resources Utilization of Xinjiang Production and Construction Corps, Shihezi 832003, China

[4]Geography Science College, Taiyuan Normal University, Taiyuan 030000, China

*to whom all correspondence should be addressed: e-mail: 15899292069@163.com

GRAPHICAL ABSTRACT

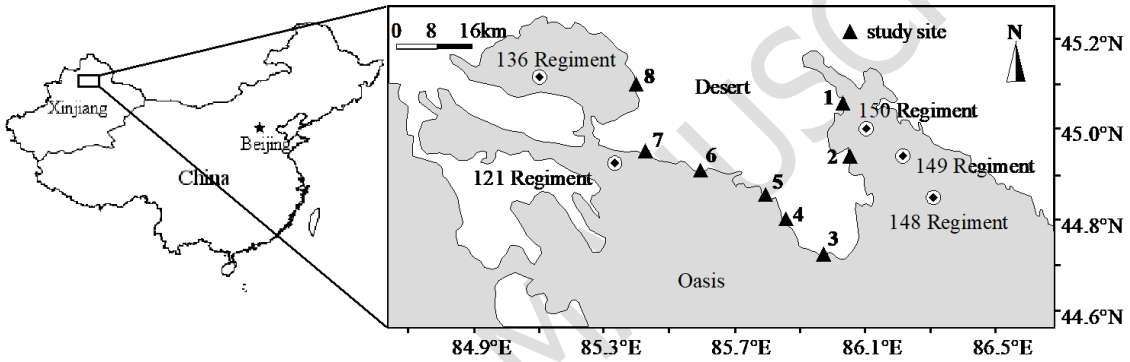

Abstract

Wind erosion is mainly a phenomenon of arid and semiarid areas, and the porosity of shelterbelts is an important quantitative index for estimating windbreak structure. However, there appears to be considerable variation in the optimal degree of porosity. With the example of an oasis–desert ecotone in Junggar Basin, the physical mechanisms responsible for wind erosion were used to investigate the optimal porosity of shelterbelts for wind speed reduction and a mathematical model relating porosity of shelterbelts to relative wind speed was constructed. The results show significant correlation among total shelterbelt porosity, crown area, average crown height, and average clear bole height (r^2 = 0.968, p = 0.000). A sharp inflection point was found near a porosity of 0.35 based on the emission mechanisms. Both emission mechanisms and the mathematical model showed that the optimal porosity of shelterbelts is between 0.35 and 0.37, confirming the results of previous research.

Keywords: oasis–desert ecotone, shelterbelt, porosity, wind erosion, wind speed reduction

1. Introduction

Wind erosion is mainly a phenomenon of arid and semiarid areas (Pimentel and Kounang, 1998; Shao, 2008). It not only affects regional environment and climate change but also results in wind–sand disasters (Shao et al., 2003; Andreae & Rosenfeld, 2008; Lv & Dong, 2012; He et al., 2017). The core of an anti-desertification project is changing the characteristics of a surface that is vulnerable to erosion. Reducing wind velocity and particle transport rate are keys to controlling wind erosion. Shelterbelts or windbreaks play a vital role in reducing damage from wind. The wind flow modification of a particular shelterbelt or multiple shelterbelt systems is dependent on its structure,

characterized by width, length, shape, and porosity (Santiago *et al.*, 2007; Van Thuyet *et al.*, 2014; Zheng *et al.*, 2016).

Porosity is defined as the ratio of pore space to the space occupied by tree stems, branches, twigs, and leaves and affects the degree of wind speed reduction as well as the shelter extent behind the windbreak (Naegeli, 1953; Raine & Stevenson, 1977; Lampartova *et al.*, 2015). Porosity of shelterbelts is not only a quantitative index for estimating windbreak structure and an important parameter for characterizing windbreak structure but also one of the most important parameters with respect to the extent and magnitude of the shelter effect (Hagen *et al.*, 1981; Wang & Takle, 1995; Guan *et al.*, 2002; Lee *et al.*, 2014; Wu *et al.*, 2018).

Jiang *et al.* (1999) reported the largest wind speed reduction when the porosity reached 0.25. Cao (1983) reported the largest windproof effect of shelterbelts when the porosity reached 0.25–0.4. Ferreira (2011) employed computational and experimental approaches to study the structural design of a natural windbreak and found a porosity of 0.35 for the shortest row in a rectangular shape. However, there appears to be considerable variation in the optimal degree of porosity. The optimal porosity range was generally in agreement with previous studies: 19% for coniferous tree shelterbelt (Grant and Nickling, 1998); 30% (Lee *et al.*, 2002) or 35% (Santiago *et al.*, 2007) for fence model in wind tunnel; 20–35% for forest models in wind tunnel (Cornelis and Gabriels, 2005); and several synthesis analyses (Okin *et al.*, 2006; Ian *et al.*, 2009). For researchers, this variation suggests the difficulty of quantifying the relationship between shelterbelts and wind erosion to determine the optimal porosity (Okpoli, 2019), (Edson and Rapheal, 2020), (Ademila *et al.*, 2019), (Okpoli and Iselowo, 2019).

Large areas of shelter forests and natural vegetation are distributed in an oasis–desert transitional zone, an important area for reducing wind and stabilizing sand in the western arid zone of China (Kang *et al*., 2018; Liu and Liu, 2010; Liu, 2018). Shelter forests and natural vegetation can play an essential role in preventing desert advance and maintaining the ecological security of oases. In the present study, the physical mechanisms responsible for wind erosion were used to investigate the optimal porosity of shelterbelts for wind speed reduction. To test the simulation results, a mathematical model relating shelterbelt porosity to relative wind speed was constructed.

2. Materials and Methods

2.1. Study sites

An oasis–desert ecotone (44°49′15.76″–45°06′19.17″N, 85°09′27.94″–86°13′33.92″E) in the southern marginal zone of the Junggar Basin in Xinjiang was selected as our study area (Fig. 1). It has an arid climate with an average annual temperature of 5–5.7 °C, evaporation of 2,000–2,800 mm, strong winds for 25–77 days of the year, wind velocity of 2–3.6 m/s, precipitation of 80–190 mm, sunlight hours of 2,700–3,050, and annual precipitation from April to June of 29–58 mm. Thus, this region exhibits a typical arid and semiarid continental climate with long, cold winters and dry, windy springs. The natural vegetation of the oasis–desert ecotone was dominated by shrubs (such as *Calligonum mongolicum*, *Tamarix ramosissima*, and *Artemisia halodendron*). *Haloxylon ammodendron* acted as its construction species, and there were large differences among the indices of species richness and species diversity and evenness in different regions (Xu *et al.*, 2012). The tree species constitutions of the shelterbelts were relatively simple, and most were pure forest. Most tree species of the pure forest were *Poplars*. Seventeen rows of shelterbelts were surveyed, of which 12 were pure forest and five were mixed forest. Two rows of mixed forests were mixtures of *Elms* and *Elaeagnus*, and others were mixtures of *Elms* and *Poplars*.

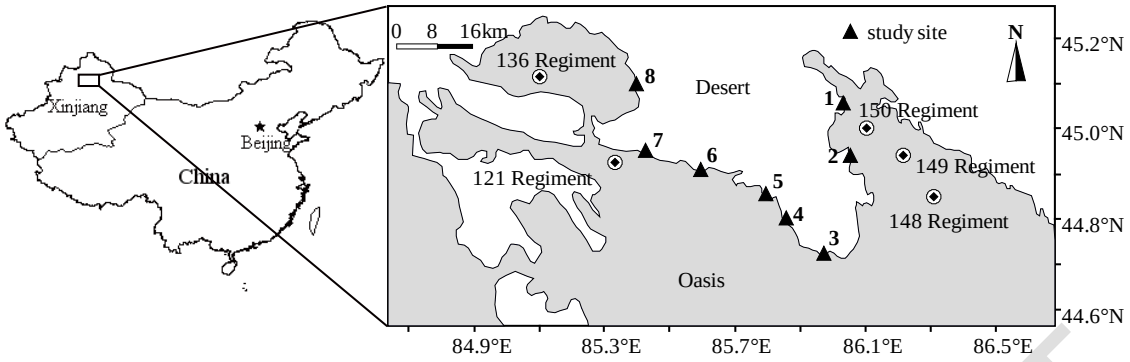

Figure 1. Distribution diagram of the experimental samples.

2.2. Data collection

According to the different habitat types of vegetation, eight experimental samples were established in an oasis–desert ecotone in the Mosowan and Xiayedi regions of the Basin. According to the shelterbelt length, shelterbelt structure, and peripheral natural vegetation coverage, we selected different numbers and structures of forest belts of the same shelterbelt as research subjects at each study site. The shelterbelts are described in Table 1.

Table 1. The characteristics of shelterbelt segments and prevalent wind direction in sample plots during the experiment

Shelterbelts segments	Study sites	Species	rows	Lengths (m)	Widths (m)	Spacing (m^2)	Porosity	Prevailing direction
1	1	*Poplars*	2	213.62	1.76	3.52	0.1511	Desert→Oasis
2	2	*Poplars*	6	315.71	15.48	7.74	0.1361	Desert→Oasis
3	2	*Poplars*	5	228.53	14.45	7.88	0.1433	Desert→Oasis
4	3	*Poplars*	2	444.76	1.83	3.66	0.4458	Oasis→Desert
5	3	*Poplars*	2	257.36	1.58	3.16	0.4957	Oasis→Desert
6	4	*Elms, Elaeagnus*	4	306.45	10.72	5.36	0.2753	Oasis→Desert
7	4	*Elms, Elaeagnus*	5	296.36	11.15	5.68	0.2542	Oasis→Desert
8	5	*Poplars*	6	346.27	15.36	7.68	0.307	Oasis→Desert
9	5	*Poplars*	6	296.84	15.42	7.72	0.324	Oasis→Desert
10	5	*Poplars*	5	274.24	14.98	7.63	0.3406	Oasis→Desert
11	6	*Poplars*	2	313.48	3.48	3.61	0.5412	Oasis→Desert
12	6	*Poplars*	2	406.83	3.57	3.73	0.5374	Oasis→Desert
13	6	*Poplars*	2	416.33	3.79	3.59	0.5116	Oasis→Desert
14	7	*Elms, Poplars*	8	398.42	22.52	8.52	0.165	Oasis→Desert
15	7	*Elms, Poplars*	8	468.34	22.34	8.36	0.1738	Oasis→Desert
16	7	*Elms, Poplars*	7	472.57	22.23	8.23	0.1872	Oasis→Desert
17	8	*Poplars*	6	278.53	15.92	7.95	0.3721	Oasis→Desert

According to the shelterbelt length and other indicators, the study selected different structures of forest belt and surveyed the structures of the forest belt using the methods described by Guan *et al.* (2002). In detail, a 50-m forest belt was selected near the center of the shelterbelt as the study sample; dead trees were counted to calculate survival rates; the perimeter method was used to measure DBH; crown

width was estimated visually; mean height, mean height under branches, and mean crown height were measured digitally; and tree species, row numbers, row spacing, in-row spacing, lengths, and widths were recorded. For rapid and accurate quantitative measurement on shelterbelt porosity, windbreak porosity was measured digitally (Guan *et al.*, 2002), (Kamel and Sana, 2019), (Ali and Vinod, 2020), (Mohammad et al., 2020), (Ismail et al., 2019).

Soil samples were collected at a depth of 0–10 cm with three replicates at each site. Each site was divided into five positions (two points in front and behind and one point inside the tree belt), and mean values were calculated. Soil particle size, soil moisture content, and electrolytic conductivity were measured following Zhao *et al.* (2010).

There were two measurement points along the prevailing wind direction at each site. One point was selected on the side near the oasis, 300–400 m from the shelterbelt. The wind speed at this point was used as a control to represent the wind speed in open areas (El-Sayed and Mohamed, 2018). The other point was selected on the desert side of the shelterbelt, 400–500 m from the shelterbelt. There was no vegetation near the measuring point, which was located in a flat area. The wind speed at this point was compared with that at the control point to estimate the windbreak effect. Wind speed was measured with an AVM-03 anemometer (with accuracy ± 3% ± 0.1 when the unit is $m \cdot s^{-1}$) at different heights (0.5 and 1.5 m). At each study site, two plots were selected at 10-m vertical intervals in the prevailing wind direction to reduce the measurement error. The data were recorded for 30 min and the mean of 60 readings recorded at 20-s intervals was used.

The relative wind speed was used to describe the reduction and was calculated by the following equation (Bijay *et al.*, 2010): $RV(\%) = U/U_0 \times 100\%$, where RV is the relative wind speed, U is the wind speed on the lee side of the shelterbelt, and U_0 is the wind speed at the control point measured at the same time as U. The windbreak effect is calculated as $100\% - RV$.

2.3. The physical mechanisms responsible for wind erosion

Previous research has shown that threshold friction velocity is affected by factors such as grain size distribution, soil moisture content, and salt content of the surface soil, and by the presence and characteristics of surface roughness elements. For soils with a mean particle size of d, u_{*t} is given by the following equation (1) (Lv & Dong, 2012):

$$u_{*t}(d) = \sqrt{A_N\left(\sigma_p g\ d + \frac{\varepsilon}{\rho d}\right)} \times \sqrt{1 + k\ w} \times e^{a\ s} \times \sqrt{(1 - m\ a\lambda)(1 + m\beta\ \lambda)} \quad (1)$$

where A_N is a proportionality coefficient (0.0123) that depends on the particle friction Reynolds number, δ_p is the particle-to-air density ratio, g is the acceleration due to gravity (9.8 m s^{-2}), d is the mean diameter of the particles (m), $\mathcal{E}$ is a coefficient (3×10^{-4}) (Shao *et al.*, 1996), w is the soil moisture content, k is a correction factor that accounts for the effect of grain size (Dong *et al.*, 2002), e is the base of natural logarithms, a is an empirical coefficient that ranges from 0.1 to 0.2, s is the soil salt content (Nickling & Ecclestone, 1981), and m is 0.16 for typical vegetation roughness elements (Raupach *et al.*, 1993). α is the ratio of basal to frontal area for the roughness elements, $\beta = Cr/Cs$, where Cr and Cs are the drag coefficients of an individual roughness element and of the smooth surface, respectively (Shao *et al.*, 1996). This study used an equation proposed by Shao (1996) to calculate the frontal area (λ) representing the roughness density, using the vegetation cover as calculated from the survey data sets: $\lambda = npA/s$, where n is the number of roughness elements in a

surface area of *s*, *p* is the porosity of roughness elements, and *A* is the mean lateral area of the roughness element.

2.4. The calculation of streamwise sand flux

By definition, the streamwise sand flux (*Q*) is the vertically integrated sand drift intensity per unit of time and breadth. For soil with a uniform partical size (*d*), *Q* is given by the following equation (2) (Owen, 1964):

$$Q(d)=\begin{cases}\dfrac{C_0\rho_a u_*^3}{g}\left[1-\left(\dfrac{u_{*t}(d)}{u_*}\right)^2\right] & u_*>u_{*t}(d)\\ 0 & u_*\le u_{*t}(d)\end{cases} \quad (2)$$

Where C_0 is a constant of order unity, ρ_a is the air density, u_* is the friction velocity.

3. Results

3.1. A dominant-factors model relating porosity to other structural factors

First, using one-way ANOVA and standard error analysis, we determined that using Photoshop and a digital camera allowed us to make a digitized measurement of porosity that is exact and credible, with standard error 0.01–0.06.

In addition, we established a dominant-factors model via stepwise regression between porosity and other structural factors of shelterbelts (Singh *et al*., 2018). Porosity was the dependent variable and other structural factors the independent variables, as follows: width (*W*), number of rows (*N*), row spacing (*Z*), line spacing (*I*), spacing ($Q = Z \times I$), average bole height (*P*), average height (*H*), relative bole height ($X = P/H$), average crown height (*J*), average crown width (*K*), average crown length (*C*), canopy area ($S = K \times C$), canopy volume ($V = S \times J$), and logarithm of cross-sectional area at breast height (lnG). Porosity and other structural factors were analyzed by stepwise regression analysis, and the regression equation (3, 4) was as follows:

$$\beta = 0.033P - 0.016J - 0.002S + 0.398 \ (r2 = 0.968, p = 0.000) \quad (3)$$

$$\beta = 0.048P - 0.016H - 0.002S + 0.398 \ (r2 = 0.968, p = 0.000) \quad (4)$$

We found significant correlations among total porosity, crown area, and the averages of crown and clear bole height ($r^2 = 0.968$, $p = 0.000$). To test the reliability of the model, the regression equation was analyzed and the results are shown in Figures 2 and 3.

The residuals of the shelterbelt porosity model followed a normal distribution with mean zero. The variance was homogeneous and the maximum absolute value of a standardized residual was 2.016. The results showed that the sample has no singular value (Fig. 2). Paired *t* test ($r = 0.982$, $p = 0.582 > 0.05$) showed that the simulated results agree well with the test results (Fig. 3).

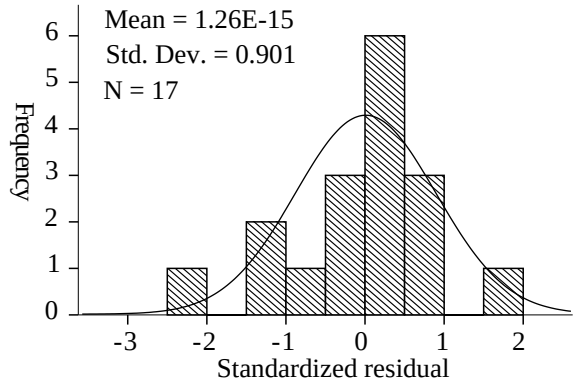

Figure 2: Histogram of standardized residuals of porosity regression

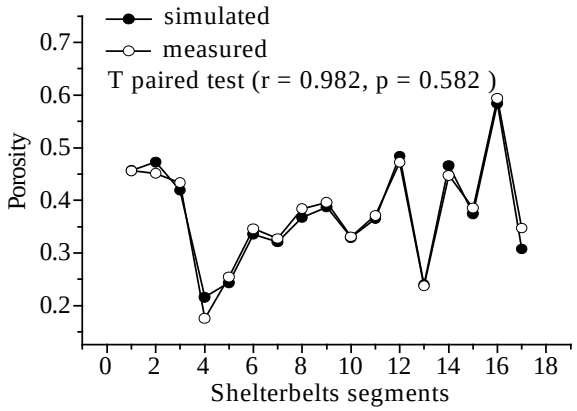

Figure 3. Comparison of simulated and measured values of porosity

3.2. Variation in optimal shelterbelt porosity

$R(\lambda)$ describes the sheltering effect provided by surface roughness elements, and can be determined based on the results of research by Raupach *et al.* (1993): $R(\lambda) = (1 - m\alpha\lambda)^{-1/2} (1 + m\beta\lambda)^{-1/2}$, where λ is the frontal area index, λ = npA/s, and p is the effective porosity of shelterbelts. The study used the methods of Lv & Dong (2012): for a surface covered by shelterbelts, 50 levels of porosity were chosen for model development (1, 2, 3, …, 50%). For evaluating the ability of shelterbelts to control erosion, the E index of Shen (2005) was used. When E = 1, the corresponding porosity of shelterbelts represents the optimal values. The result shows that the sheltering effect of shelterbelts decreases with increasing porosity and that there is an obvious inflection point near 35% porosity (Fig. 4). Thus, the effectiveness of shelterbelts decreases slowly with increasing porosity when the porosity is <0.35, and their effectiveness decreases rapidly with increasing porosity when the porosity is >0.35. The optimal porosity of shelterbelts is 0.35.

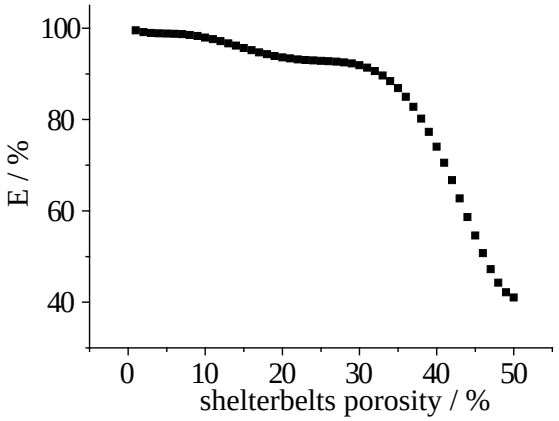

Figure 4. Variation in optimal shelterbelt porosity based on E index as a function of porosity

3.3. Analysis of the relationship between porosity and relative wind speed

To determine the effect of shelterbelt porosity on wind speed reduction, the relationships between porosity and relative wind speed at different heights (0.5 and 1.5 m) were analyzed. Because the analytical results identified the optimal porosity, the windbreak effect was analyzed. The shelterbelt direction was rarely perpendicular to the prevailing wind direction, and if the angles between the shelterbelt and wind direction are not 90°, it will affect the windbreak effect. To identify an accurate relationship, wind velocity (V) was decomposed into two components: $V_{vertical}$ and $V_{parallel}$, as shown in Fig. 5.

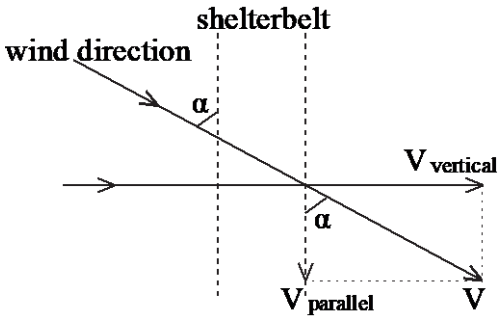

Figure 5. Effects of angles between shelterbelt and wind direction on shelter porosity

$V_{vertical} = V \sin a$ and $V_{parallel} = V \cos a$; thus, the effect of $V_{vertical}$ on the windbreak effect is greater than that of $V_{parallel}$. The relationships between porosity and $V_{vertical}$ at different heights (0.5 and 1.5 m) were analyzed. The results are shown in Fig. 6.

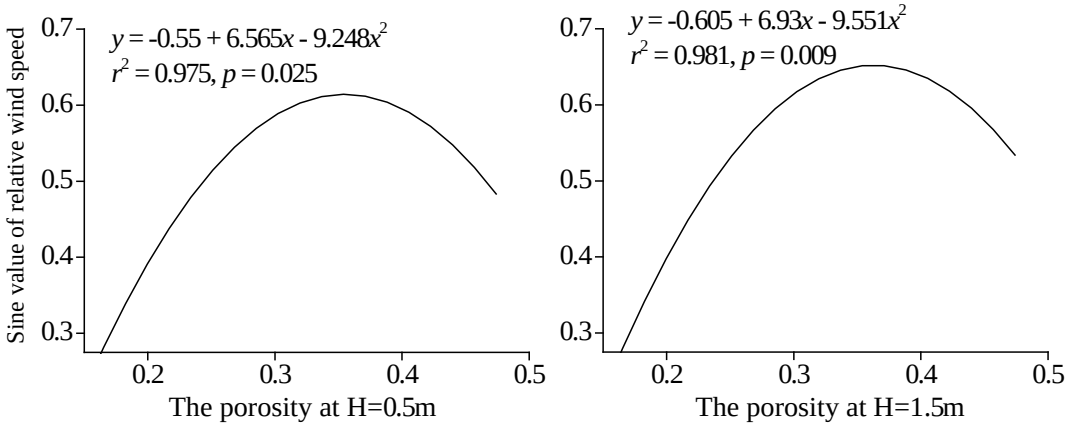

Figure 6. The functional relationship between porosity and the sine component of relative wind speed at two heights

The functional relationship between porosity and the sine component of relative wind speed at two heights is a parabolic function relationship (Fig. 6). Significance testing of the functional relationship showed significant effects at 0.5 m ($r^2_{0.5}$ = 0.975, p = 0.025) and 1.5 m ($r^2_{1.5}$ = 0.981, p = 0.009). Figure 6 also shows that the windbreak effect increases with porosity within a limit and decreases when the porosity exceeds the limit.

4. Discussion

There was an optimal porosity of shelterbelts. The derivative method was used to compute the extrema of the equation. When $dy_{0.5}/dx = 0$, $x = 0.3549$, and when $dy_{1.5}/dx = 0$, $x = 0.3628$ (Fig. 6). Thus, the optimal porosity of shelterbelts is between 0.35 and 0.37. When the porosity is between 0.35 and 0.37, the windbreak effect is 61.6% at a height of 0.5 m and 65.2% at 1.5 m. Zhu *et al.* (2002) reported that when the porosity is 0.25, the wind speed reduction is between 9% and 75% in the range of a 5–35-m height of the tree. The results of this study fall within this range.

The physical mechanisms responsible for wind erosion were used to study the optimal porosity of shelterbelts for wind speed reduction. To test the simulation results, a mathematical model relating the porosity of shelterbelts to relative wind speed was constructed. The results showed that the optimal porosity of shelterbelts is between 0.35 and 0.37. Jiang *et al.* (1999) reported the largest wind speed reduction when the porosity reached 0.25. Cao (1983) reported the largest windproofing effect of shelterbelts when the porosity reached 0.25–0.4. Ferreira (2011) employed computational and experimental approaches to study the structural design of a natural windbreak and found that the porosity was 0.35 for the shortest row of rectangular shape. Overall, the optimal porosity of this study was consistent with the results of previous research.

5. Conclusion

In the present study, the physical mechanisms responsible for wind erosion were used to study the optimal porosity of shelterbelts for wind speed reduction. A mathematical model relating the porosity of shelterbelts to relative wind speed was constructed and the effective porosity of shelterbelts at different wind speeds was established. Because the system error and human error of testing results of shelter forests shelterbelts porosity were smaller. In this study, the digitized measurement of windbreak porosity combining a digital camera and software for remote sensing image processing was developed. The results show that the process is simple and convenient, its application is wide, and it can be used to measure windbreak porosity accurately and rapidly. Significant correlations were found among total shelterbelt porosity, crown area, and the averages of crown and clear bole height. The optimal porosity of shelterbelts is between 0.35 and 0.37. Based on emission mechanisms, a clear inflection point was found near a porosity of 0.35. The inflection point near 0.35 is very important for shelterbelt control of erosion. Both emission mechanisms and the mathematical model showed that the optimal porosity of shelterbelts is between 0.35 and 0.37, confirming the results of previous research.

Acknowledgments

This project was supported by the National Natural Science Foundation of China (Grant No. 31760239) and the Key Technology R&D Program (Grant No. 2014BAC14B02). The authors would like to thank Wei Chen for the English language review. We thank Enago for its linguistic assistance during the preparation of this manuscript.

References

Ademila, O., Okpoli, C.C. and Ehinmitan, D. (2019), Geological and Lithological Mapping Of Part Of Igarra Schist Belt Using Integrated Geophysical Methods. *Earth Sciences Pakistan*, 1-9.

Ali K. and Vinod K. (2020), Spatial distribution and potential ecological risk assessment of heavy metals in agricultural soils of Northeastern Iran, *Geology, Ecology, and Landscapes*, **4**(2), 87-103.

Andreae M.O. and Rosenfeld D. (2008), Aerosol–cloud–precipitation interaction Part 1: The nature and sources of cloud-active aerosols. *Earth–Sci Rev*, **89**(1–2), 13–41.

Bijay T., Michael G.A. and Donald L.R. (2010), Microclimate patterns on the leeside of single–row tree windbreaks during different weather conditions in Florida farms: Implications for improved crop production. *Agroforest Syst***, 79**(1), 111–122.

Cao X. (1983), Farmland shelterbelt science. China Forestry Publishing House, Beijing, China.

Cornelis W.M. and Gabriels D. (2005), Optimal windbreak design for wind-erosion control. *J Arid Environ*, **61**, 315–332.

Dong Z., Liu X. and Wang X. (2002), Wind initiation thresholds of the moistened sands. *Geophys Res Lett*, **29**(12), 25–28.

Edson T. and Rapheal W. (2020), A Comparative Study of Two Biological Monitoring Systems In Assessing Water Quality: A Case Of River Birira, Sheema District, Uganda. *Water Conservation and Management*, **4**(1), 07-14.

El-Sayed S.A. and Mohamed M.K.E. (2018), Mechanical properties and characteristics of wheat straw and pellets. *Energy & Environment*, **29**(7), 1224-1246.

Ferreira A.D. (2011), Structural design of a natural windbreak using computational and experimental modeling. *Environ Fluid Mech*, **11**(5), 517–530.

Grant P.F. and Nickling W.G. (1998). Direct field measurement of wind drag on vegetation for application to windbreak design and modelling. *Land Degrad Dev*, **9**, 57–66.

Guan W., Li C., Li S., Fan Z. and Xie C. (2002), Improvement and application of digitized measure on shelterbelt porosity. *Chin J Appl Ecolo*, **13**(6), 651–657.

Hagen J.L., Skidmore E.L., Miller P.L. and Kipp J.E. (1981), Simulation of effect of wind barriers on airflow. *T ASABE*, **24**(1), 1002–1008.

He Y., Jones P.J. and Rayment M. (2017), A simple parameterisation of windbreak effects on wind speed reduction and resulting thermal benefits to sheep. *Agr Forest Meteorol*, **239**, 96-107.

Ian N., Brendan G. and Reid R. (2009), Aerodynamic and microclimate changes behind windbreaks. Agroforestry for Natural Resource Management, CSIRO Publishing, Collingwood, Australia, 78–79.

Ismail N.M., Ismail A.F., Mustafa A., Zulhairun A.K., Aziz F., Bolong N. and Razali A.R. (2019), Polymer Clay Nanocomposites for Gas Separation: A Review. *Environmental Contaminants Reviews*, **2**(1), 01-05.

Jiang F., Zhu J. and Zhou X. (1999), Model of continuous economic effects of shelterbelts or windbreaks and its applications. *Sci Sil Sin*, **35**(1), 16–21.

Kamel K. and Sana B. (2019), Spatial Variability of Soil Erodibility At El Hammam Catchment, Northeast of Algeria. *Environment & Ecosystem Science*, **3**(1), 17-25.

Kang L., Du H.L., Du X., Wang H.T., Ma W.L., Wang M.L. and Zhang F.B. (2018), Study on dye wastewater treatment of tunable conductivity solid-waste-based composite cementitious material catalyst. *Desalination and Water Treatment*, **125**, 296-301.

Lampartova I., Schneider J., Vyskot I., Rajnoch M. and Litschmann T. (2015), Impact of protective shelterbelt microclimate characteristics. *Ekológia* (Bratislava), **34**, 101–110.

Lee J., Lee E. and Lee S. (2014), Shelter effect of a fir tree with different porosities. *J Mech Sci Technol*, **28**(2), 565–572.

Lee S.J., Park K.C. and Park C.W. (2002), Wind tunnel observations about the shelter effect of porous fences on the sand particle movements. *Atmos Environ*, **36**, 1453–1463.

Liu H. and Liu Z. (2010), Recycling utilization patterns of coal mining waste in China. *Resources Conservation and Recycling*, **54**(12), 1331-1340.

Liu Z. (2018), Economic analysis of energy production from coal/biomass upgrading; Part 1: Hydrogen production. Energy Sources Part B-Economics Planning and Policy, **13**(2), 132-136.

Lv P. and Dong Z. (2012), Study of the windbreak effect of shrubs as a function of shrub cover and height. *Environ Earth Sci*, **66**(7), 1791–1795.

Mohammad S.S., Mohiuddin K. M., Laith K.T.A.A., Mohamad N.H., Rojina A., Md. Sakhawat H. and Md. Niuz M.K. (2020), Effect of Bio-Nematicide And Bau-Biofungicide Against Root-Knot (Meloidogyne Spp.) Of Soybean. *Malaysian Journal of Sustainable Agriculture*, **4**(2), 44-48.

Naegeli W. (1953), Untersuchungen über die windverhältnisse im bereich von schilfrohrwänden [Investigations on the wind conditions in the range of narrow walls of reed.] *Mitt Schweiz Anst Forstl Versuchswesen*, **29**, 213–266.

Nickling W.G. and Ecclestone M. (1981), The effects of soluble salts on the threshold shear velocity of fine sand. *Sedimentology*, **28**(4), 505–510.

Okin G.S., Gillette D.A. and Herrick J.E. (2006), Multi-scale controls on and consequences of aeolian processes in landscape change in arid and semi-arid environments. *J Arid Environ*, **65**, 253–275.

Okpoli C.C. (2019), High Resolution Magnetic Field Signatures Over Akure And Its Environs, Southwestern Nigeria. *Earth Sciences Malaysia*, **3**(1), 09-17.

Okpoli C.C. and Iselowo D.O. (2019), Hydrogeochemistry Of Lekki, Ajah And Ikorodu Water Resources, Southwestern Nigeria. *Journal Clean WAS*, **3**(2), 20-24.

Owen P.R. (1964), Saltation of uniform grains in air. *J Fluid Mech*, **20**(2), 225–242.

Pimentel D. and Kounang N. (1998), Ecology of soil erosion in ecosystems. Ecosystems, **1**(5), 416–426.

Raine J.K. and Stevenson D.C. (1977), Stevenson Wind protection by model fences in a simulated atmospheric boundary layer. *J Wind Eng Ind Aerod*, **2**(2), 159–180.

Raupach M., Gillette A. and Leys J. (1993), The effect of roughness elements on wind erosion threshold. *J Geophys Res*, **98**(D2), 3023–3029.

Santiago J.L., Martin F., Cuerva A., Bezdenejnykh N. and SanzAndres A. (2007), Experimental and numerical study of wind flow behind windbreaks. *Atmos Environ*, **41**, 6406–6420.

Shao Y. (2008), Physics and modeling of wind erosion. Kluwer Academic Publishers, Dordrecht, The Netherlands.

Shao Y., Raupach M.R. and Leys J.F. (1996), A model for predicting aeolian sand drift entrainment on scales from paddock to region. *Aust J Soil Res*, **34**(2), 309–342.

Shao Y., Yang Y., Wang J., Song Z., Leslie L.M., Dong C., Zhang Z., Lin Z., Kanai Y., Yabuki S. and Chun Y. (2003), Northeast Asian duststorms: Real–time numerical prediction and validation. *J Geophys Res*, **108**(D22), doi: 10.1029/2003JD003667.

Shen Y. (2005), Calculation and numerical simulation of sand and dust emissions by wind erosion in Northwest China. Doctoral Thesis. Graduate University of the Chinese Academy of Sciences, Beijing, China.

Singh G., Jain V.K. and Singh A. (2018), Adaptive network architecture and firefly algorithm for biogas heating model aided by photovoltaic thermal greenhouse system. *Energy & Environment*, **29**(7), 1073-1097.

Van Thuyet D., Van Do T., Sato T. and Thai Hung T. (2014), Effects of species and shelterbelt structure on wind speed reduction in shelter. *Agroforest Syst*, **88**(2), 237–244.

Wang H. and Takle E.S. (1995), A numerical simulation of boundary-layer flows near shelterbelts. *Bound–Lay Meteorol*, **75**(1–2), 141–173.

Wu T., Zhang P., Zhang L., Wang J. and Wang G. (2018), Relationships between shelter effects and optical porosity: a meta-analysis for tree windbreaks. *Agr Forest Meteorol*, **259**.

Xu M., Liu T., Zhao X. and Zhang W. (2012), Study on the collaborative windbreak effect and optimization configuration model of shelterbelt and natural vegetation in an oasis–desert ecotone in Junggar basin. *J Desert Res*, **32**(5), 1224–1232.

Zhao H., Liu T., Lei J., Gui D. and Zhao X. (2010), β diversity characteristic of vegetation community on south part of Gurbantunggut Desert and its interpretation. Acta Pratacul Sin **19**(3): 29–37.

Zheng X., Zhu J. and Xing Z. (2016), Assessment of the effects of shelterbelts on crop yields at the regional scale in Northeast China. Agr Syst **143**: 49-60.

Zhu J., Jiang F. and Matsuzaki T. (2002), Spacing interval for principal tree windbreaks. *J Forest Res-Jpn*, **13**(2), 83–90.